

Electronic Supplementary Material (ESI) for Journal of Materials Chemistry A

Electrochemical Formation of PtRu bimetallic Nanoparticles for Highly Efficient and pH-Universal Hydrogen Evolution Reaction

Lu Li⁺, Gengwei Zhang⁺, Bin Wang, Tao Yang^{*} and Shengchun Yang^{*}

L. Li, G.W. Zhang, B. Wang, T. Yang*, Prof. S.C. Yang*

Key Laboratory of Shanxi for Advanced Materials and Mesoscopic Physics

State Key Laboratory for Mechanical Behavior of Materials

School of Science

Xi'an Jiaotong University

Xi'an 710049, People's Republic of China

E-mail: ysch1209@mail.xjtu.edu.cn. (S. Yang), taoyang1@mail.xjtu.edu.cn (T. Yang)

Lu Li and Gengwei Zhang contribute equally to this work

Experimental

1.1 Reagents:

Ruthenium trichloride (RuCl_3) was obtained from the Kunming institute of precious metals. Trace Pt was obtained by dissolving from Pt wires. Potassium hydroxide, dipotassium hydrogen phosphate and potassium dihydrogen phosphate are all purchased from Aladdin Industrial Corporation. Deionized (DI) water (18.25 M Ω) used in experiment was prepared by passing through an ultra-pure purification system.

1.2 Catalyst Synthesis

The carbon cloth (1 cm²) was immersed in an aqueous solution containing 0.011 mol L⁻¹ RuCl_3 for 20 minutes, and then drying for 30 minutes at 60 °C followed by heating treatment at 300 °C for 20 minutes in air to obtain the RuO_2 nanocrystal loaded carbon cloth electrode (RuO_2/CC). The content of Ru loaded on the carbon cloth measured by ICP-MS was about 13.9 $\mu\text{g cm}^{-2}$. PtRu/CC₁₅₀₀ was synthesized by the ECD method, which was performed using a CHI 760E electrochemical workstation (CHI Instrument Company, Shanghai, China)¹⁻⁴ and a standard three-electrode cell containing N₂-saturated 0.5 M H_2SO_4 at room temperature. The content of Pt on the carbon cloth was measured by ICP-MS. The as-prepared RuO_2/CC sample, Pt wires and Hg/Hg₂SO₄ electrode were used as the working electrode, counter electrode and reference electrode, respectively. The ECD cycles of 500, 1000, 1500 and 2000 were carried out between -0.35 and 0.1 V versus RHE at a scan rate of 100 mV s⁻¹ for Pt electrochemical dissolution from counter electrode and then depositing on working electrode. For comparison, RuO_2/CC electrode without Pt deposition was also prepared

via the same method as the above for PtRu/CC, expect that the common electrolytic cell was replaced with an H-type electrolytic cell separated by Nafion film to prevent Pt migration, and rule out the impact of ECD process on performance. A certain volume of the 20% Pt/C ink was carefully dropped onto the carbon cloth to obtain the Pt/C catalyst with a desirable Pt loading amount of $1.6 \mu\text{g cm}^{-2}$ and $15.5 \mu\text{g cm}^{-2}$.

1.3 Electrochemical Measurements

All electrochemical measurements were performed on the CHI 760E electrochemical workstation at room temperature. For each HER experiment, cathodic linear sweep voltammetry (LSV) with the scan rate of 5 mV s^{-1} was performed in N_2 -saturated $0.5 \text{ M H}_2\text{SO}_4$, 1 M PBS and 1 M KOH solutions. The reference electrode in $0.5 \text{ M H}_2\text{SO}_4$, 1 M PBS and 1 M KOH solutions was $\text{Hg/Hg}_2\text{SO}_4$, saturated calomel and Hg/HgO electrode, respectively. A graphite rod was used as the counter electrode. Unless otherwise specified, iR correction was used of all the original data.

Prior to the performance measurement, $\text{Hg/Hg}_2\text{SO}_4$ electrode calibration was carried out in a three-electrode system in which Pt wires served as both working electrode and counter electrode, and $\text{Hg/Hg}_2\text{SO}_4$ served as the reference electrode. H_2 -saturated $0.5 \text{ M H}_2\text{SO}_4$ solution was employed as electrolyte. Linear sweep voltammetry (LSV) was then conducted in the range of -0.71 to -0.7 V at a scan rate of 1 mV s^{-1} (H_2 was still purged during measurement). The potential at which the current crosses zero was taken as the thermodynamic potential (vs. $\text{Hg/Hg}_2\text{SO}_4$) for the hydrogen electrode (Fig. S2). Thereby, all the potentials reported in our manuscript tested in $0.5 \text{ M H}_2\text{SO}_4$ solution were calibrated to a reversible hydrogen electrode

(RHE) by using the equation: $E \text{ (vs. RHE)} = E \text{ (vs. Hg}_2\text{SO}_4) + 0.7075 \text{ V}$. In the same way, we calibrated the saturated calomel (Fig. S3) and Hg/HgO electrode (Fig. S4). The potentials in 1 M PBS and 1 M KOH were calibrated to RHE by using the equation: $E \text{ (vs. RHE)} = E \text{ (vs. SCE)} + 0.65 \text{ V}$, $E \text{ (vs. RHE)} = E \text{ (vs. Hg/HgO)} + 0.928 \text{ V}$, respectively.

Cyclic voltammetry (CV) curves with various scan rates (namely, 20, 40, 60, 80 and 100 mV s^{-1}) were measured to calculate the electrochemically active surface area (ECSA), which was proportional to the double layer capacitance (C_{dl}).⁴⁻⁶ Assuming that the specific capacitance of a flat surface was $\sim 40 \mu\text{F}$ for 1 cm^2 of real surface area, then the ECSA was estimated as:

$$ECSA = \frac{C_{dl} \text{ (mF cm}^{-2}\text{)}}{40 \mu\text{F cm}^{-2} \text{ per cm}_{ECSA}^2}$$

The calculation of TOF:

To calculate the turnover frequency (TOF), CV method with the potential range of -0.2 to 0.6 V (vs. RHE) at a scan rate of 50 mV s^{-1} was performed in 1.0 M PBS.⁶⁻⁹ When the number of active sites was determined, the TOF was calculated with the equation:

$$TOF = \frac{I}{2nF} \quad (1)$$

Where I was the current (in A) for different samples during the LSV measurements in 0.5 M H_2SO_4 , 1 M PBS and 1.0 M KOH solutions, respectively, F was the Faraday constant (in C/mol), and n was the number of active sites (in mol) for different samples.

The number of active sites was measured from CV curves within the potential range of -0.2 to 0.6 V (vs. RHE) at a scan rate of 50 mV s⁻¹ in 1.0 M PBS (pH=7). With a given geometric area A , the number of active sites n is proportional to the charge Q , which can be calculated from the obtained CV curve by integrating. Therefore,

$$I_{cv} = J_{cv} \cdot A \quad (2)$$

$$t = \frac{U_{cv}}{\nu} \quad (3)$$

$$Q = \frac{1}{2} \int d(I_{cv}t) = \frac{1}{2} \int d\left(\frac{U_{cv}}{\nu} J_{cv}\right) = \frac{1}{2} \int \frac{1}{\nu} d(U_{cv} J_{cv} A) = \frac{A}{2\nu} \int dU_{cv} J_{cv} = \frac{SA}{2\nu} \quad (4)$$

Because the charge Q of surface active site (n) can be described by $Q = nF$, therefore,

$$n = \frac{SA}{2\nu F} \quad (5)$$

Where I_{cv} , J_{cv} , U_{cv} are the current, current density, and potential obtained from CV curve, ν is the scan rate, S is the integrated area of CV curve.

Thus, TOF is calculated by this equation:

$$TOF = \frac{I}{2nF} = \frac{I}{2 \frac{SA}{2\nu F}} = \frac{\nu I}{SA} = \frac{J\nu}{S} \quad (6)$$

Where J is the current density in LSV curves, ν is the scan rate (50 mV s⁻¹ in this work), and S is the integrated areas of CV curves.

The Faradaic efficiency was calculated by comparing the measured and theoretically produced amounts of H₂.

1.4 Computational Models and Methods

All spin-polarized density functional theory (DFT) calculations were performed by using the Vienna Ab Initio Simulation Package (VASP)¹⁰. The generalized-gradient approximation with the form of PBE¹¹ was used as the correlation and exchange energy functional. The vdW correction was considered by employing the Grimme's D3¹² scheme because of the dispersion interaction of adsorption water systems. To describe the interactions between valence electrons and the ion core, the projector augmented wave (PAW) method was adopted.¹³ The energy cut-off energy for the plane wave basis set was chosen as 400 eV. The convergence criteria for the electronic structure and geometry relaxation were 10^{-5} eV and 0.02 eV/Å, respectively. For hexagonal close-packed (hcp) Ru and face center cubic (fcc) Pt unitcell, a $9 \times 9 \times 9$ Monkhorst-Pack mesh¹⁴ were used as K-point. The optimized lattice parameters of Ru unitcell ($a = b = 2.690$ Å, $c = 4.245$ Å) and Pt unitcell ($a = b = c = 3.914$ Å) agree well with the experimental values of Ru ($a = b = 2.706$ Å, $c = 4.282$ Å)¹⁵ and Pt ($a = b = c = 3.924$ Å)¹⁶. For hydrogen adsorption, the Pt(111) and Ru(101) surfaces were modeled by three-layered 2×2 supercell and 1×2 supercell, respectively (Fig. S30), in which the top two atomic layers are allowed to relax while the bottom one is fixed, in order to compare with the previous calculations. A $5 \times 5 \times 1$ Monkhorst-Pack mesh was used to sample the first Brillouin zone in the surface calculations. In the case of H₂O adsorption, the Pt(111) and Ru(101) surfaces were modeled by three-layered 4×4 supercell and 2×3 supercell, respectively, as shown in Fig. S31. A $3 \times 3 \times 1$ Monkhorst-Pack mesh was used to sample the first Brillouin zone in the surface calculations. A vacuum

spacing of 15 Å was added in the z-direction without a dipole correction to avoid the interaction between the slab and its repeated motif. The calculations of isolated small molecules were performed by using a (10 Å × 10 Å × 10 Å) unit cell with the Γ -point only for the k-point sampling.

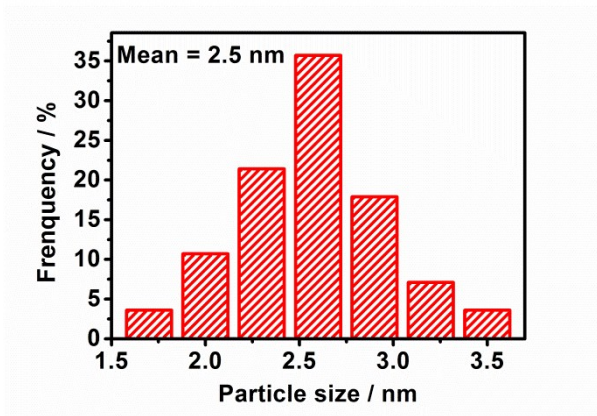


Fig. S1 Histogram of diameter distribution of the sample after 1500 ECD cycles.

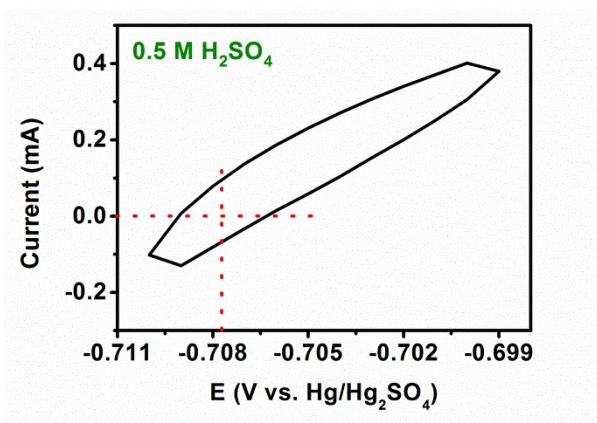


Fig. S2 Hg/Hg₂SO₄ reference electrode calibration curve in 0.5 M H₂SO₄ solution.

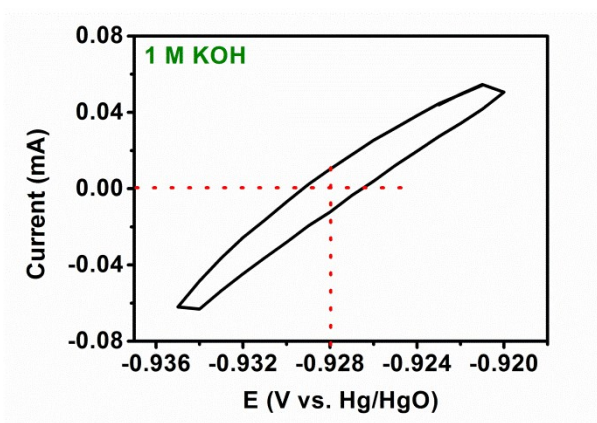


Fig. S3 Hg/HgO reference electrode calibration curve in 1 M KOH solution.

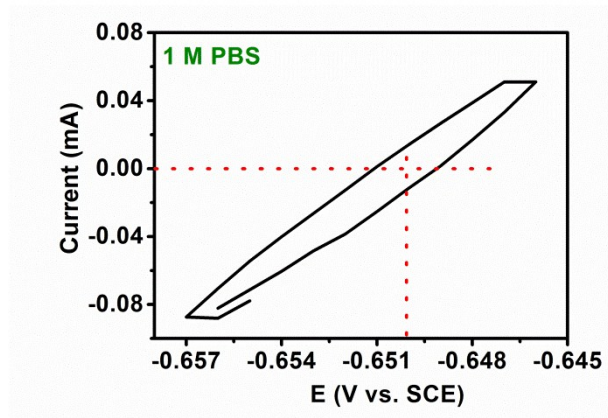


Fig. S4 saturated calomel reference electrode calibration curve in 1 M PBS.

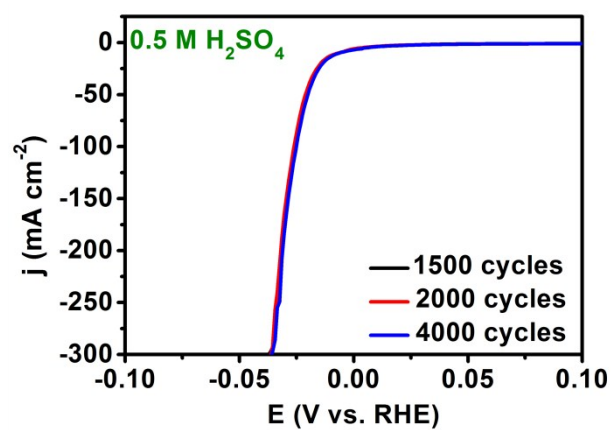


Fig. S5 HER polarization curves of the RuO₂/CC after 1500, 2000 and 4000 ECD cycles in 0.5 M H₂SO₄ solution.

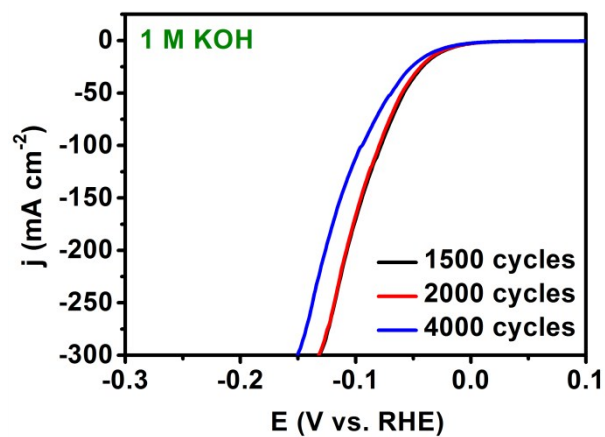


Fig. S6 HER polarization curves of the RuO₂/CC after 1500, 2000 and 4000 ECD cycles in 1.0 M KOH solution.

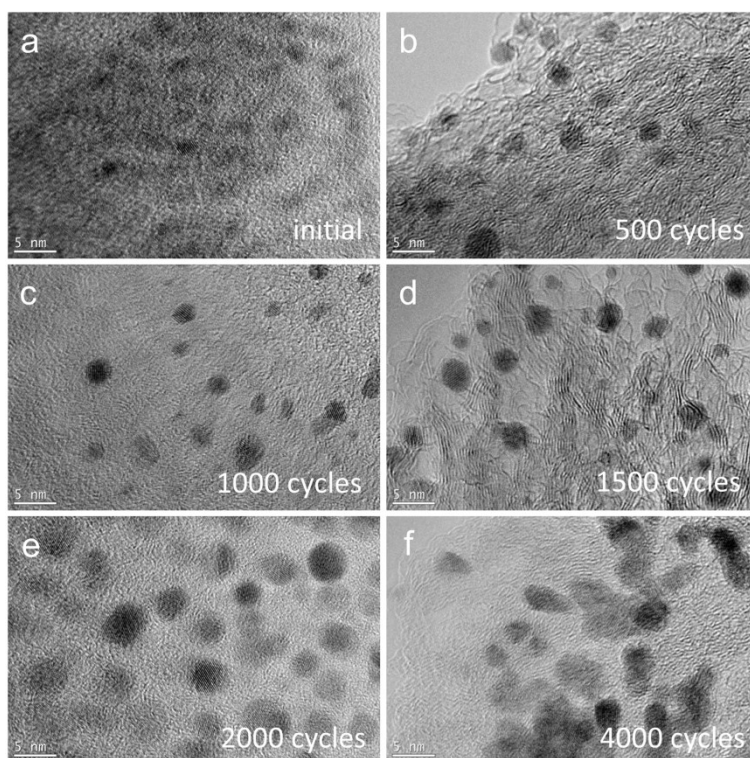


Fig. S7 Morphology of the sample during ECD process: (a) initial, (b) 500 cycles, (c) 1000 cycles, (d) 1500 cycles, (e) 2000 cycles and (f) 4000 cycles.

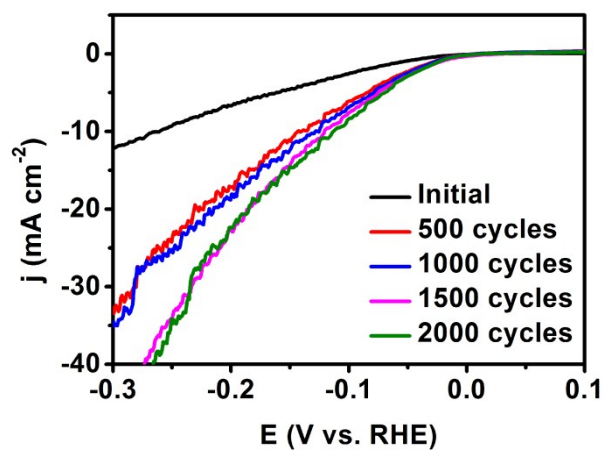


Fig. S8 HER polarization curves of the bare CC after 0, 500, 1000, 1500 and 2000 ECD cycles in 0.5 M H₂SO₄ solution.

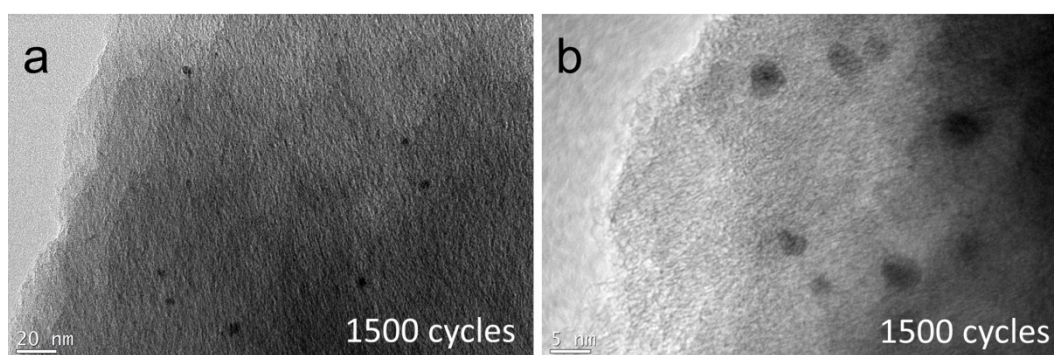


Fig. S9 TEM images of the bare CC after 1500 ECD cycles.

Table. S1 The loading mass of Ru and Pt during ECD process measured by ICP-MS.

sample	Ru ($\mu\text{g cm}^{-2}$)	Pt ($\mu\text{g cm}^{-2}$)
initial	14	0
500 cycles	14.05	≈ 0
1000 cycles	13.42	0.445
1500 cycles	13.95	1.605
2000 cycles	14.1	4.5

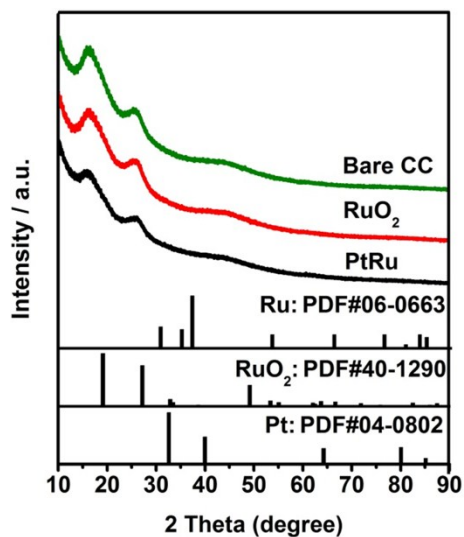


Fig. S10 XRD pattern of bare CC, RuO₂/CC and PtRu/CC₁₅₀₀.

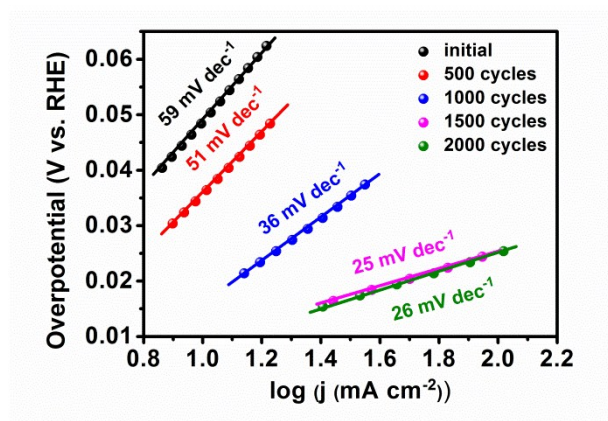


Fig. S11 Tafel plots at different ECD cycles.

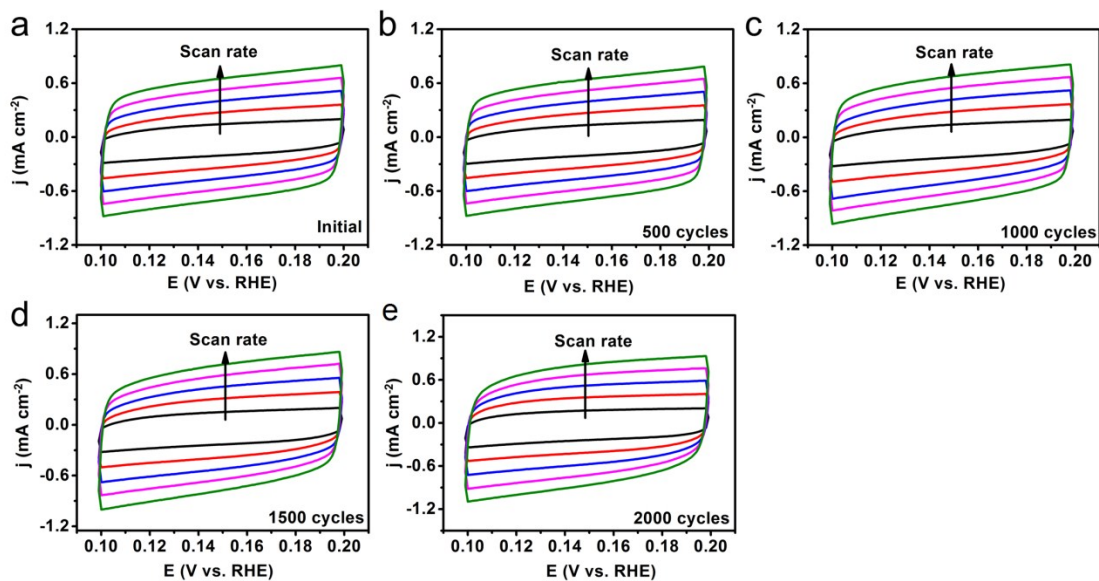


Fig. S12 CVs of the sample during ECD process: (a) initial, (b) 500 cycles, (c) 1000 cycles, (d) 1500 cycles and (e) 2000 cycles.

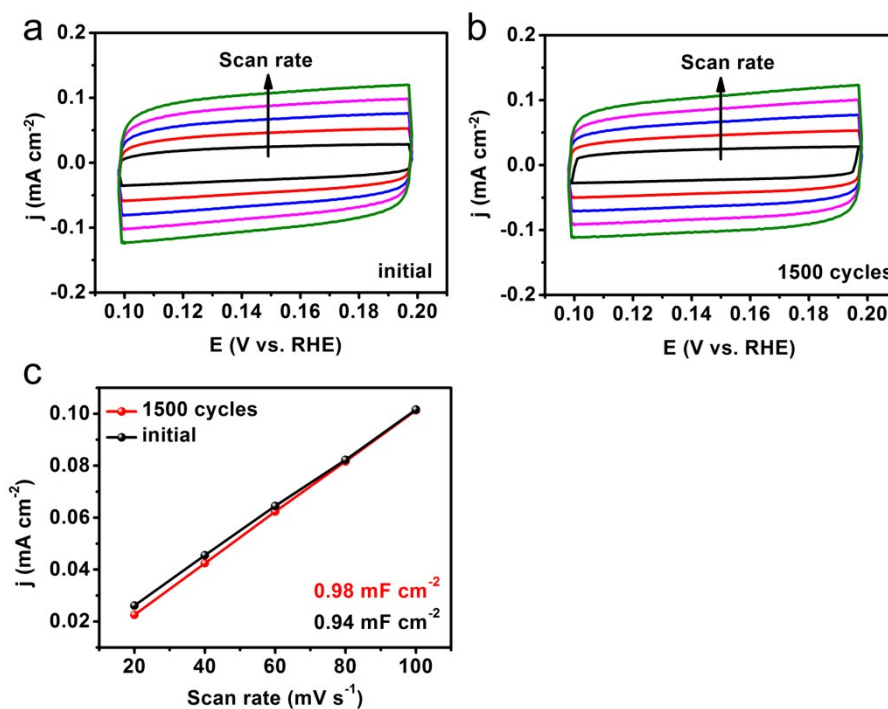


Fig. S13 CVs of the bare CC during ECD process: (a) initial, (b) 1500 cycles, and (c) double-layer capacitance (C_{dl}).

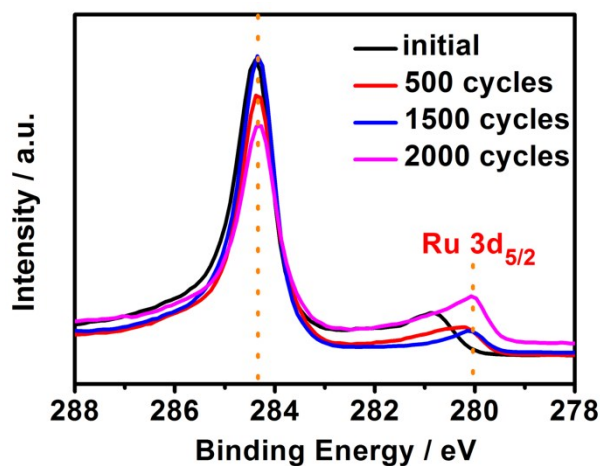


Fig. S14 The change of Ru 3d_{5/2} XPS spectrum during ECD process.

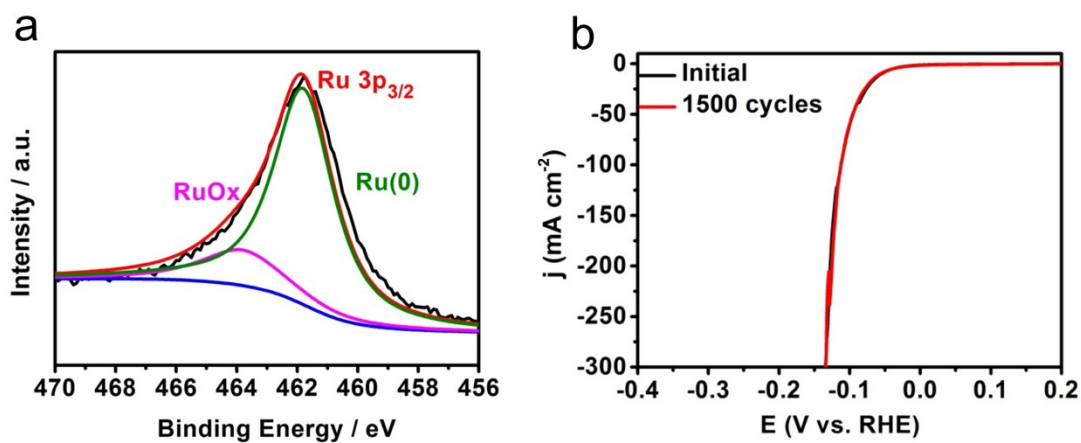


Fig. S15 Characterization of the RuO₂/CC sample after CV treatment with 1500 cycles in H-type electrolytic cell. a) the corresponding Ru 3p XPS spectrum, b) the HER polarization curves for above sample at initial and after 1500 ECD cycles in 0.5 M H₂SO₄ solution.

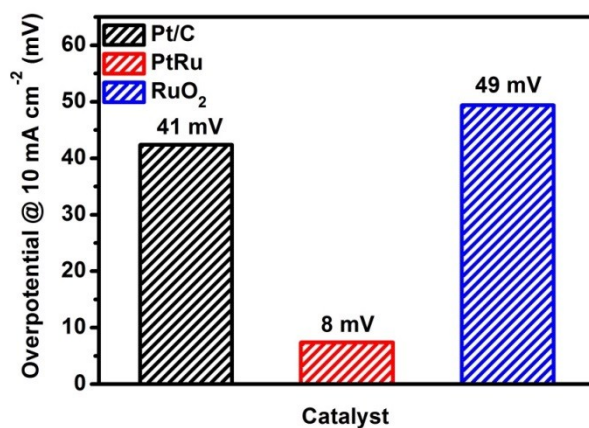


Fig. S16 Overpotentials at 10 mA cm⁻² of commercial Pt/C, PtRu/CC₁₅₀₀ and RuO₂ in N₂-saturated 0.5 M H₂SO₄ solution.

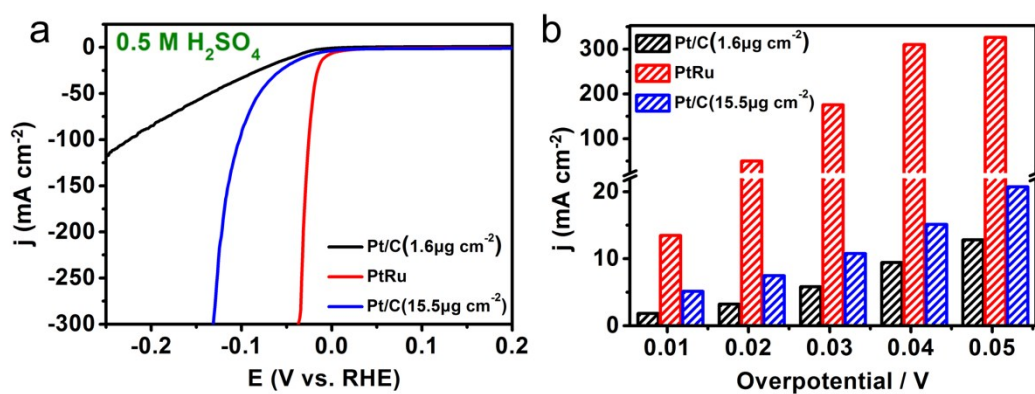


Fig. S17 a) HER polarization curves and b) current densities at special overpotential of commercial Pt/C (with Pt loading amount of 1.6 μg cm⁻² and 15.5 μg cm⁻² respectively) and PtRu/CC₁₅₀₀ in 0.5 M H₂SO₄ solution.

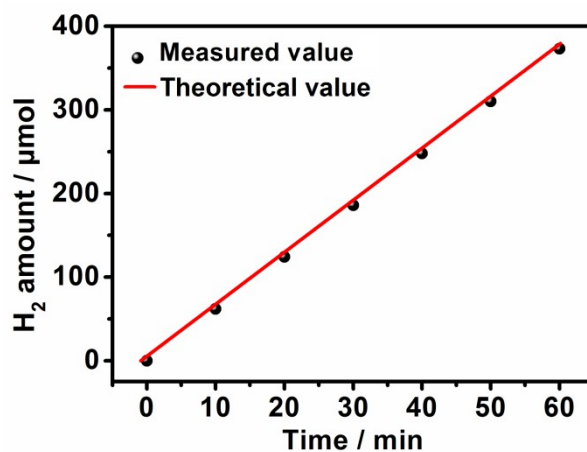


Fig. S18 Faradic efficiency of H_2 generation over $\text{PtRu}/\text{CC}_{1500}$ electrode at a current of 20 mA for 60 minutes.

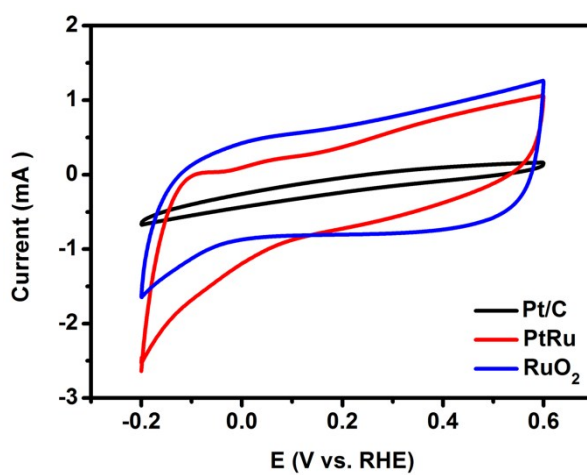


Fig. S19 CVs of as-prepared samples in phosphate buffer solution at a scan rate of 50 mV s^{-1} .

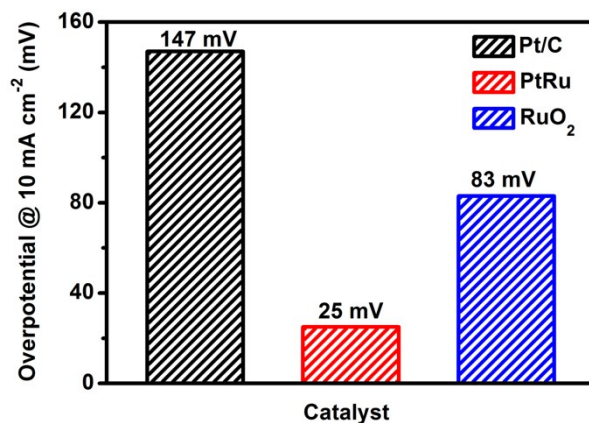


Fig. S20 Overpotentials at 10 mA cm⁻² of Pt/C, PtRu/CC₁₅₀₀ and RuO₂/CC in N₂-saturated 1 M PBS.

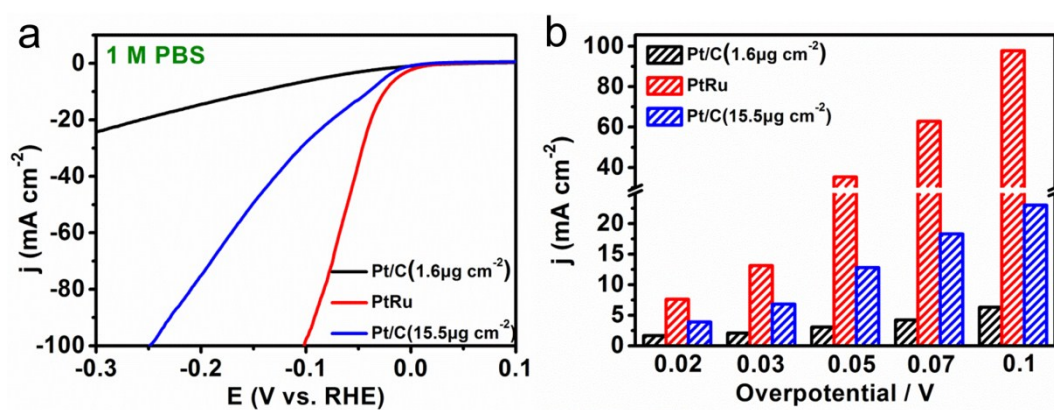


Fig. S21 a) HER polarization curves and b) current densities at special overpotential of commercial Pt/C (with Pt loading amount of 1.6 μg cm⁻² and 15.5 μg cm⁻² respectively) and PtRu/CC₁₅₀₀ in 1 M PBS.

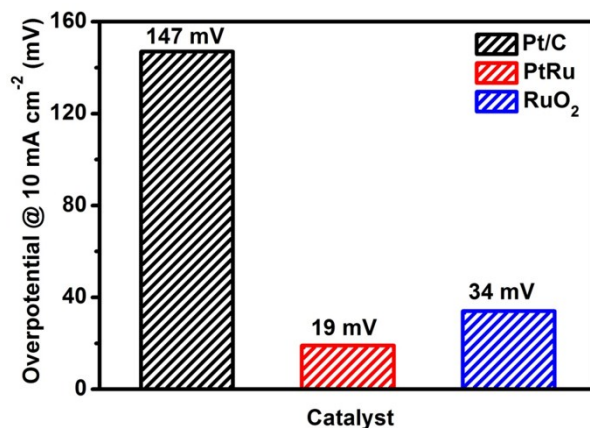


Fig. S22 Overpotentials at 10 mA cm⁻² of Pt/C, PtRu/CC₁₅₀₀ and RuO₂/CC in N₂-saturated 1 M KOH solution.

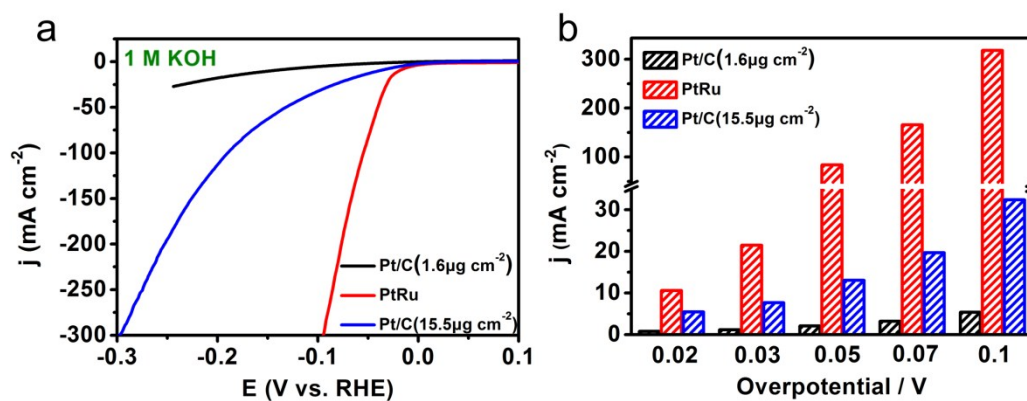


Fig. S23 a) HER polarization curves and b) current densities at special overpotential of commercial Pt/C (with Pt loading amount of 1.6 μg cm⁻² and 15.5 μg cm⁻² respectively) and PtRu/CC₁₅₀₀ in 1 M KOH solution.

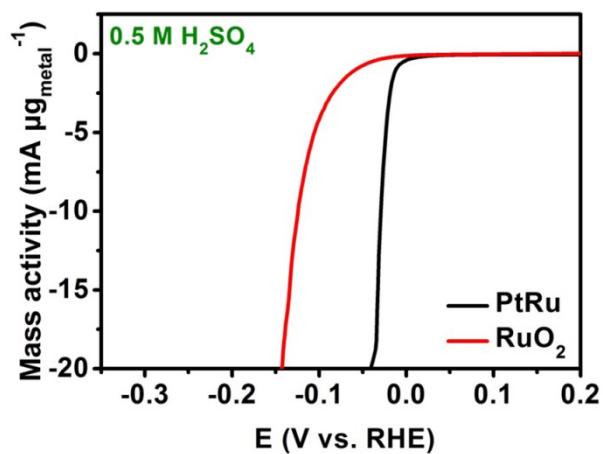


Fig. S24 Mass activity of PtRu/CC₁₅₀₀ and RuO₂/CC in 0.5 M H₂SO₄ solution normalized by the loading amount of total metal.

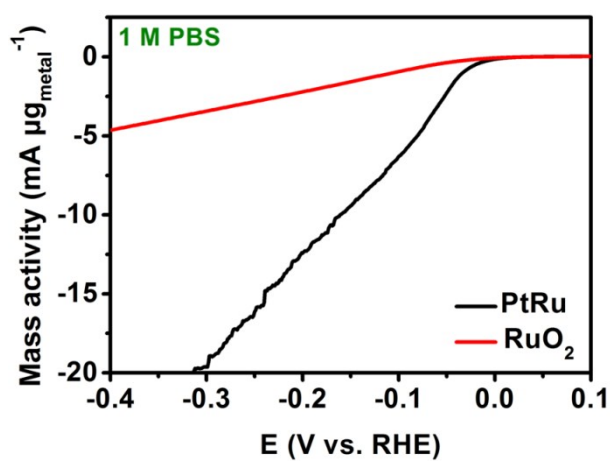


Fig. S25 Mass activity of PtRu/CC₁₅₀₀ and RuO₂/CC in 1 M PBS normalized by the loading amount of total metal.

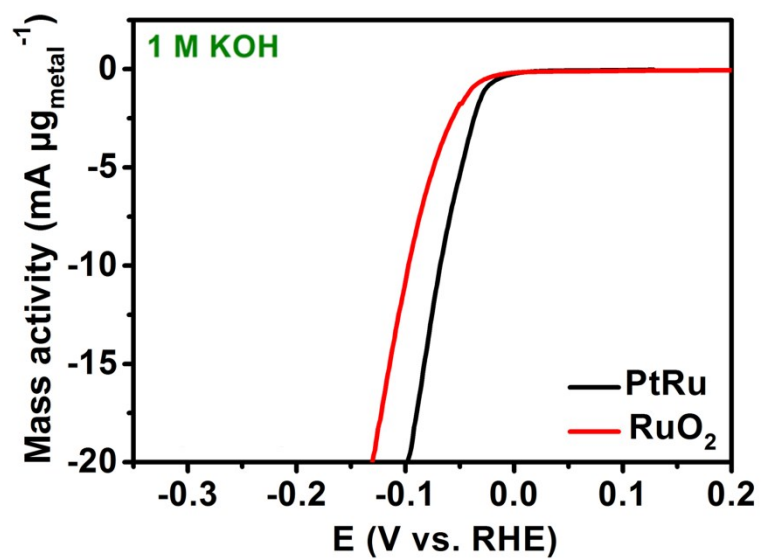


Fig. S26 Mass activity of PtRu/CC₁₅₀₀ and RuO₂/CC in 1.0 M KOH normalized by the loading amount of total metal.

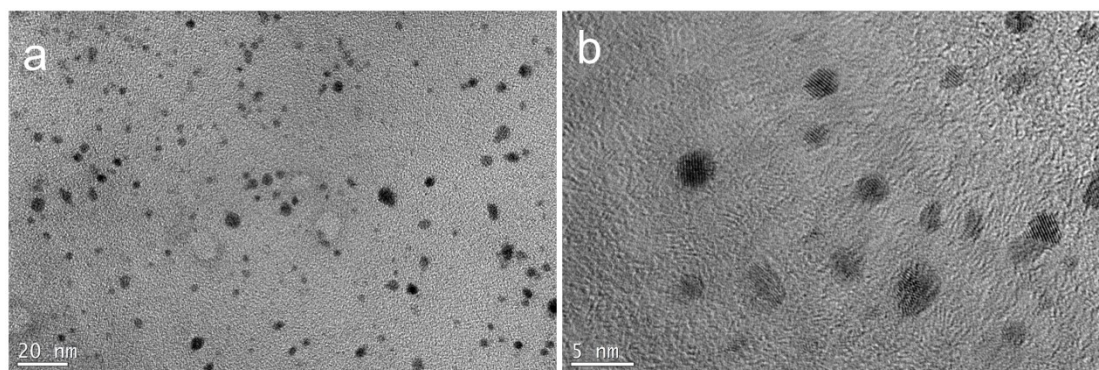


Fig. S27 Morphological characterization of post-HER for the PtRu/CC₁₅₀₀. (a) large-area TEM image, (b) TEM image.

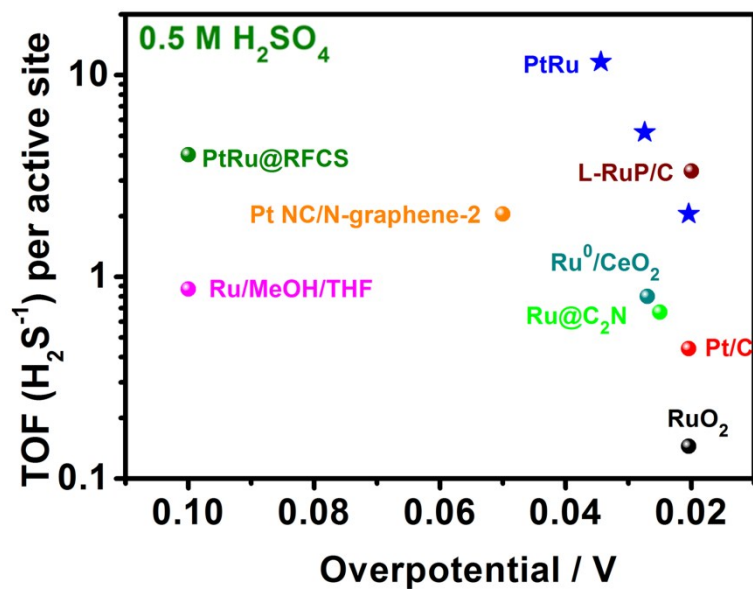


Fig. S28 TOF values of PtRu/CC₁₅₀₀, with other recently reported noble metal HER electrocatalysts in 0.5 M H₂SO₄ solution.

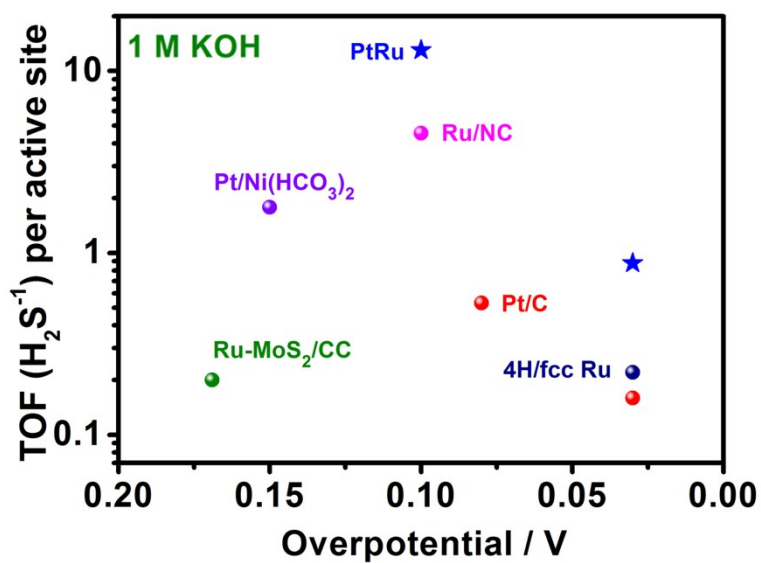


Fig. S29 TOF values of PtRu/CC₁₅₀₀, with other recently reported noble metal HER electrocatalysts in 1 M KOH solution.

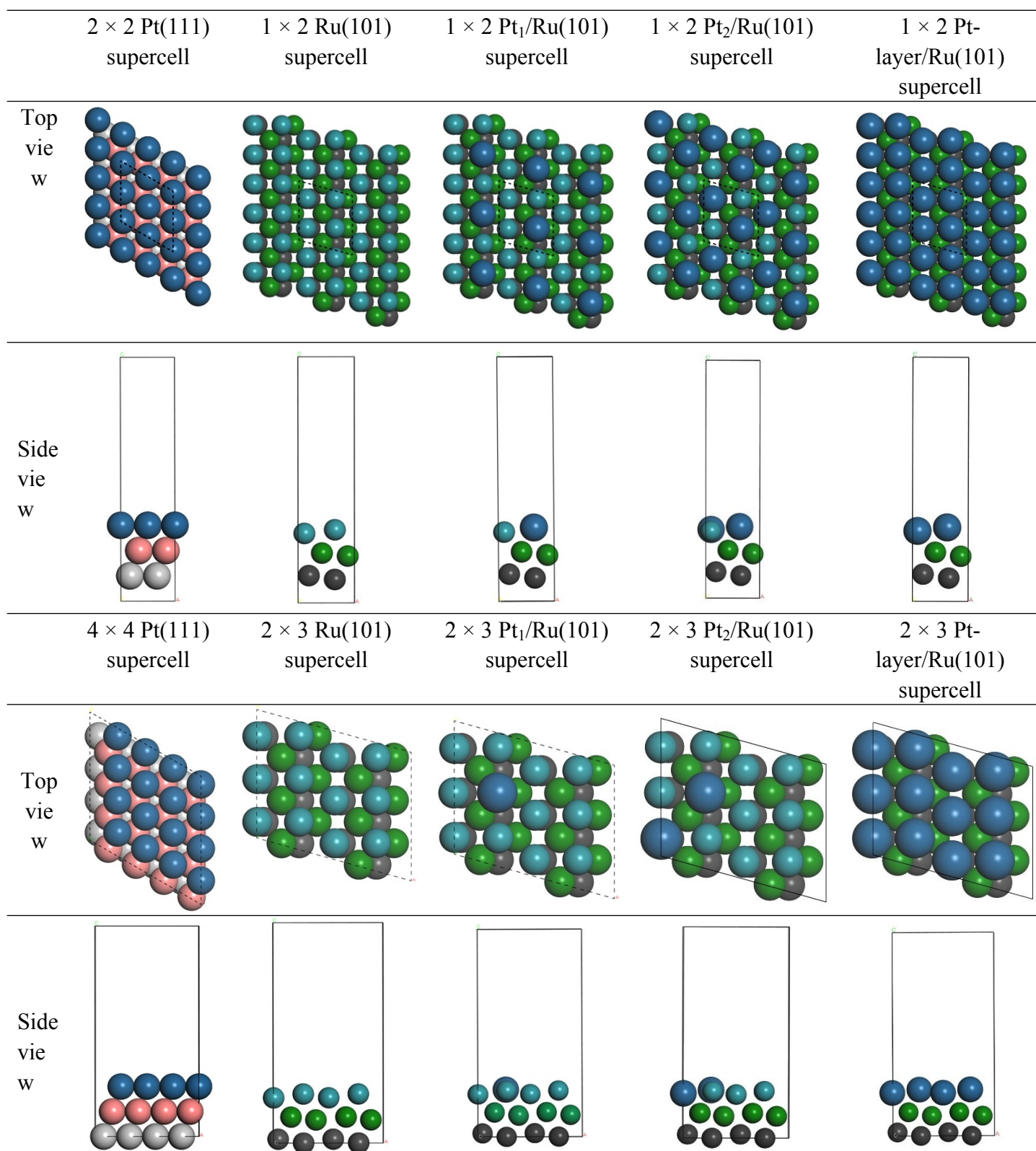


Fig. S30 Top (top) and side (bottom) view of three metal surfaces, including Pt(111) surface, Ru(101) surface, Pt₁/Ru(101) surface, Pt₂/Ru(101) surface, and Pt-layer/Ru(101) surface. The top, middle, and bottom layers of those models were colored by different colors.

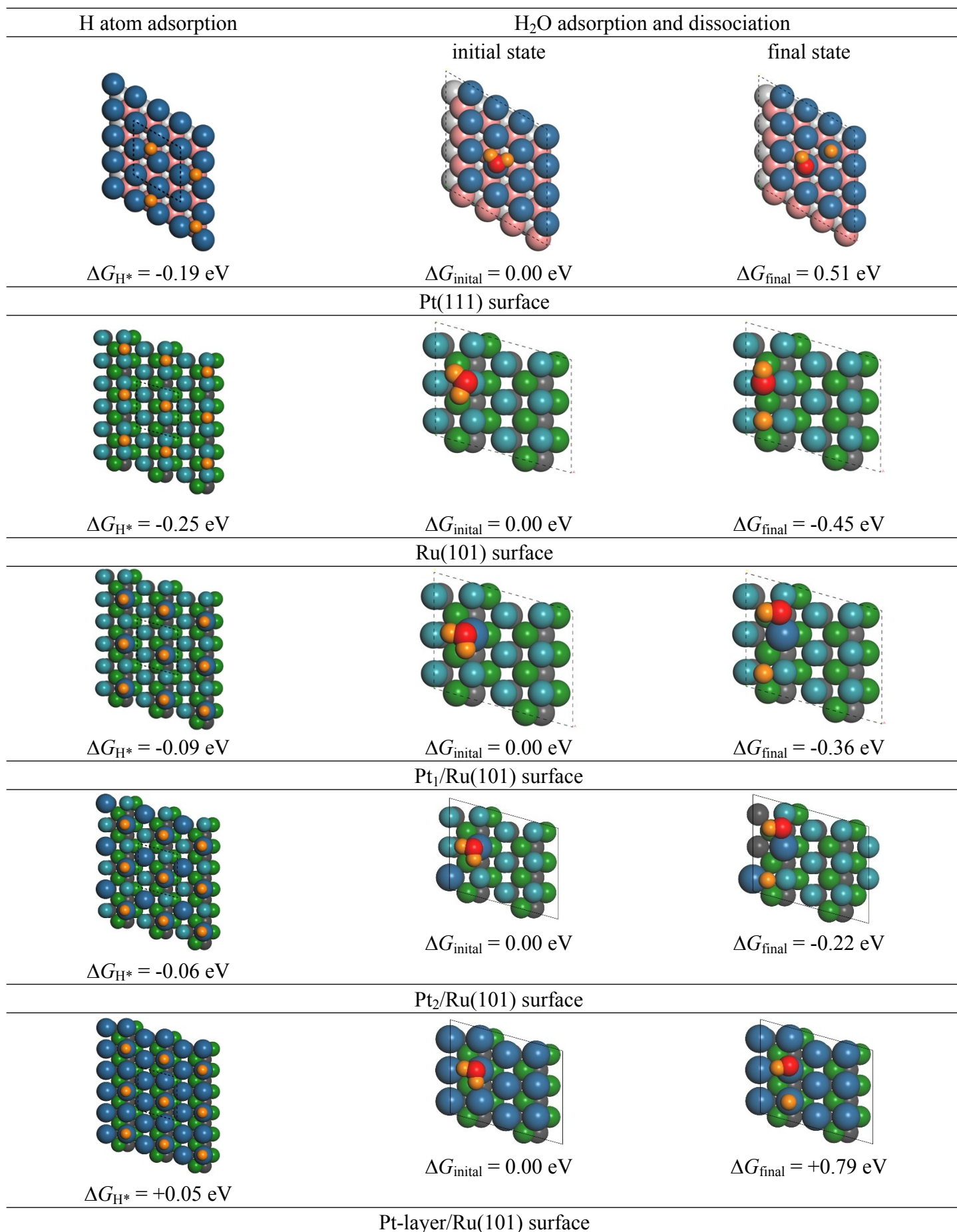


Fig. S31 H atom and H₂O adsorption and dissociation on three metal surfaces, including Pt(111) surface, Ru(101) surface, Pt₁/Ru(101) surface, Pt₂/Ru(101) surface, and Pt-layer/Ru(101) surface. Yellow and red balls represent hydrogen and oxygen atoms, respectively.

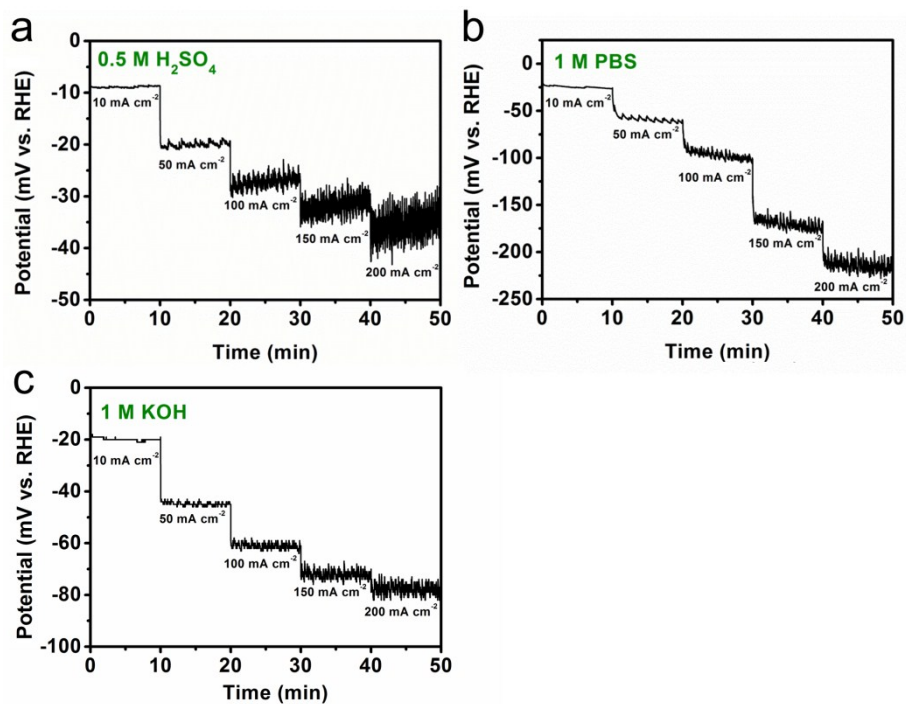


Fig. S32 Steady-state chronoamperometry for PtRu/CC₁₅₀₀ in 0.5 M H₂SO₄, 1 M PBS and 1 M KOH, respectively.

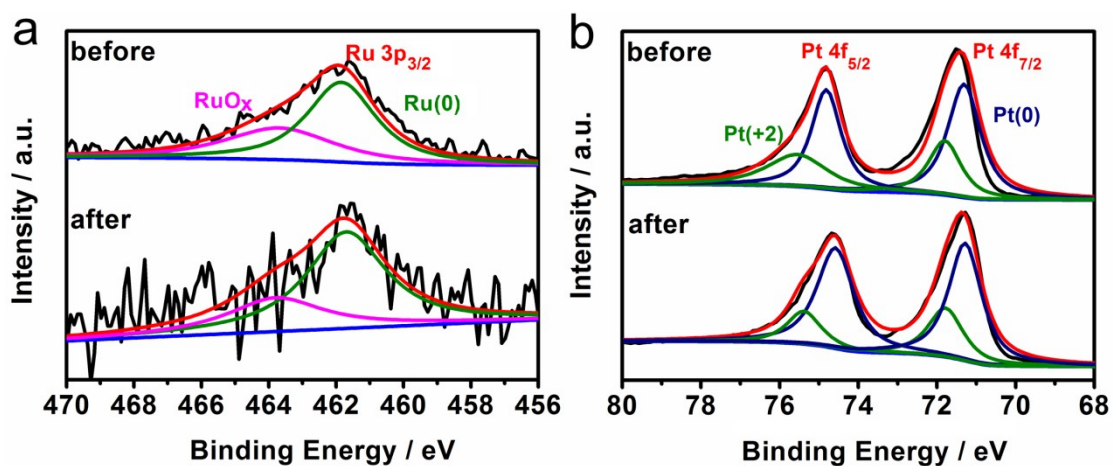


Fig. S33 XPS for PtRu/CC₁₅₀₀ before and after long-term HER testes. (a) Ru 3p spectrum, (b) Pt 4f spectrum.

Table S2 Summary of some recently reported representative HER electrocatalysts in acidic electrolytes. *The value is evaluated from the polarization curves exhibited in the literature.

catalyst	electrolyte	J₀ (mA cm⁻²)	TOF (s⁻¹)	Loading (μg cm⁻²)	Tafel slope (mV dec⁻¹)	η₁₀ (mV)	ref
PtRu/CC₁₅₀₀	0.5M H ₂ SO ₄	2.44	13.35 (η=50 mV)	13.9 _{Ru} /1.6 _{Pt}	25	8	This work
RuP₂@NPC	0.5M H ₂ SO ₄	1.99	---	1000	38	38	1
Ru-MoO₂	0.5M H ₂ SO ₄	---	---	570	44	55	17
Ru/MeOH/THF	0.5M H ₂ SO ₄	----	0.87 (η=100 mV)	352	46	83	18
Ru nanosheet	0.5M H ₂ SO ₄	----	----	~100	46	(10 mA mg ⁻¹) 20	19
Ru/GLC	0.5M H ₂ SO ₄	-----	-----	400	46	35	20
Ru/NG-750	0.5M H ₂ SO ₄	-----	-----	24.2 _{Ru}	44	53	21
Ru⁰/CeO₂	0.5M H ₂ SO ₄	0.54	0.8 (η=27 mV)	197	33	41	22
PtRu@RFCS	0.5M H ₂ SO ₄	1.57	4.03 (η=100 mV)	354	27.2	19.7	5
Ru@GnP	0.5M H ₂ SO ₄	-----	-----	750	30	13	23
Ru@CN	0.5M H ₂ SO ₄	-----	----	~750	----	126	24
Ru@C₂N	0.5M H ₂ SO ₄	1.9	0.670 (η=25 mV)	285	30	13.5	25
L-RuP/C	0.5M H ₂ SO ₄	3.22	3.35 (η=20 mV)	464	37	19	26
Ru-MoS₂/CC	0.5M H ₂ SO ₄	---	----	46 _{Ru}	---	61	27
PtO_x/TiO₂	0.5M H ₂ SO ₄	----	-----	---	40	120*	28

Table S3 Summary of some recently reported representative HER electrocatalysts in neutral electrolytes.

catalyst	electrolyte	J₀ (mA cm⁻²)	TOF (s⁻¹)	Loading (μg cm⁻²)	Tafel slope (mV dec⁻¹)	η₁₀ (mV)	ref
PtRu/CC₁₅₀₀	1 M PBS	2.35	4.36 (η=100 mV)	13.9 _{Ru} /1.6 _{Pt}	36	25	This work
RuP₂@NPC	1 M PBS	----	-----	1000	87	57	1
Rh₂P	1 M PBS	-----	-----	150	46	38	29
V₈C₇	0.1 M PBS	-----	-----	1900	64	77	30
CoP/Co-MOF	1 M PBS	-----	-----	5000	63	49	31
FePSe₃/NC	1 M PBS	----	----	212	167	140.1	32
CoP@BCN-1	1 M PBS	----	-----	400	59	122	33
Ni₂P@NPCNFs	1 M PBS	----	-----	337	230.3	185.3	34
MoP/CNT	1 M PBS	1.291	----	500	109	102	35
Re₃P₄@NPVC	1 M PBS	----	----	143	77	61	36
Ni_{0.89}Co_{0.11}Se₂	1 M PBS	----	-----	2620	78	82	37

Table S4 Summary of some recently reported representative HER electrocatalysts in alkaline electrolytes.

catalyst	electrolyte	J₀ (mA cm⁻²)	TOF (s⁻¹)	Loading (μg cm⁻²)	Tafel slope (mV dec⁻¹)	η₁₀ (mV)	ref
PtRu/CC₁₅₀₀	1 M KOH	1.25	13.01 (η=100 mV)	13.9 _{Ru} /1.6 _{Pt}	28	19	This work
Ru-MoS₂/CC	1 M KOH	----	0.2 (η=169 mV)	46 _{Ru}	114	41	27
RuP₂@NPC	1 M KOH	---	----	1000	69	52	1
Ru-MoO₂	1 M KOH	----	----	285	31	29	17
Ru@GnP	1 M KOH	----	----	250	28	22	23
Ru@CN	1 M KOH	----	----	~750	53	32	24
Cu_{2-x}S@Ru	1 M KOH	----	----	230	48	82	38
NiO_x/Pt₃Ni	1 M KOH	----	----	15	----	40	39
Ru₂P	1 M KOH	----	----	380	29.3	75	40
Ru₂-GC	1 M NaOH	----	----	430	65	25	41
Ru_{0.33}Se@TNA	1 M KOH	0.73	----	200	50	57	42
4H/fcc Ru	1 M KOH	1.62	0.22 (η=30 mV)	34	29.4	23	43
Ru-Ru₂P/PC	1 M KOH	----	----	285	35.1	57	44
Ni₃N/Pt	1 M KOH	----	----	2000	36.5	50	45
Pt/Ni(HCO₃)₂	1 M KOH	----	1.78 (η=150 mV)	40	40	44	46
Ru ND/C	1 M KOH	----	----	35.4	49	43.4	47

References

1. Z. Pu, I. S. Amiin, Z. Kou, W. Li and S. Mu, *Angew. Chem.*, **2017**, 129, 11717-11722.
2. Z. Yang, C. Zhao, Y. Qu, H. Zhou, F. Zhou, J. Wang, Y. Wu and Y. Li, *Adv. Mater.*, **2019**, 31, 1808043.
3. N. Du, C. Wang, X. Wang, Y. Lin, J. Jiang and Y. Xiong, *Adv. Mater.*, **2016**, 28, 2077-2084.
4. L. Zhang, L. Han, H. Liu, X. Liu and J. Luo, *Angew. Chem. Int. Ed.*, **2017**, 56, 13694-13698.
5. K. Li, Y. Li, Y. Wang, J. Ge, C. Liu and W. Xing, *Energy Environ. Sci.*, **2018**, **11**, 1232-1239.
6. X. Shang, Z. Z. Liu, S. S. Lu, B. Dong, J. Q. Chi, J. F. Qin, X. Liu, Y. M. Chai and C. G. Liu, *ACS Appl. Mater. Inter.*, **2018**, **10**, 43561-43569.
7. W. Gao, M. Yan, H. Y. cheung, Z. Xia, X. Zhou, Y. Qin, C. Y. Wong, J. C. Ho, C. R. Chang and Y. Qu, *Nano Energy*, **2017**, **38**, 290-296.
8. C. Zhang, J. Sha, H. Fei, M. Liu, S. Yazdi, J. Zhang, Q. Zhong, X. Zou, N. Zhao, H. Yu, Z. Jiang, E. Ringe, B. I. Yakobson, J. Dong, D. Chen and J. M. Tour, *ACS Nano*, **2017**, **11**, 6930-6941.
9. G. Zhao, K. Rui, S. X. Dou and W. Sun, *Adv. Funct. Mater.*, **2018**, **28**, 1803291.
10. G. Kresse and J. Furthmüller, *Phys. Rev. B*, **1996**, 54, 11169-11186.
11. J. P. Perdew, K. Burke and M. Ernzerhof, *Phys. Rev. Lett.*, **1996**, 77, 3865 - 3868.
12. S. Grimme, J. Antony, S. Ehrlich and S. Krieg, *J. Chem. Phys.*, **2010**, 132, 154104.
13. P. E. Blöchl, *Phys. Rev. B*, **1994**, 50, 17953-17979.
14. H. J. Monkhorst and J. D. Pack, *Phys. Rev. B*, **1976**, 13, 5188-5192.
15. V. A. Finkel, M. I. Palatnik and G. P. Kovtun, *Phys. Met. Metall.*, **1971**, 32, 231.
16. Y. Waseda, K. Hirata and M. Ohtani, *High Temp. High Pressures*, **1975**, 7, 221.
17. P. Jiang, Y. Yang, R. Shi, G. Xia, J. Chen, J. Su and Q. Chen, *J. Mater. Chem. A*, **2017**, 5, 5475-5485.
18. S. Drouet, J. Creus, V. Colliere, C. Amiens, J. Garcia-Anton, X. Sala and K. Philippot, *Chem. Commun.*, **2017**, 53, 11713-11716.
19. X. Kong, K. Xu, C. Zhang, J. Dai, S. N. Oliaee, L. Li, X. Zeng, C. Wu and Z. Peng, *ACS Catal.*, **2016**, 6, 1487-1492.
20. Z. Chen, J. Lu, Y. Ai, Y. Ji, T. Adschiri and L. Wan, *ACS Appl. Mater. Inter.*, **2016**, 8, 35132-35137.
21. R. Ye, Y. Liu, Z. Peng, T. Wang, A. S. Jalilov, B. I. Yakobson, S. H. Wei and J. M. Tour, *ACS Appl. Mater. Inter.*, **2017**, 9, 3785-3791.
22. E. Demir, S. Akbayrak, A. M. Önal and S. Özkaz, *ACS Appl. Mater. Inter.*, **2018**, 10, 6299-6308.
23. F. Li, G. F. Han, H. J. Noh, I. Ahmad, I. Y. Jeon and J. B. Baek, *Adv. Mater.*, **2018**, 30, 1803676.
24. J. Wang, Z. Wei, S. Mao, H. Li and Y. Wang, *Energy Environ. Sci.*, **2018**, 11, 800-806.
25. J. Mahmood, F. Li, S. M. Jung, M. S. Okyay, I. Ahmad, S. J. Kim, N. Park, H. Y. Jeong and J. B. Baek, *Nanotechnol.*, **2017**, 12, 441-446.
26. J. Yu, Y. Guo, S. She, S. Miao, M. Ni, W. Zhou, M. Liu and Z. Shao, *Adv. Mater.* **2018**, 30, 1800047.
27. D. Wang, Q. Li, C. Han, Z. Xing and X. Yang, *Appl. Catal. B: Environ.*, **2019**, 249, 91-97.
28. X. Cheng, Y. Li, L. Zheng, Y. Yan, Y. Zhang, G. Chen, S. Sun and J. Zhang, *Energy Environ. Sci.*, **2017**, 10, 2450-2458.
29. F. Yang, Y. Zhao, Y. Du, Y. Chen, G. Cheng, S. Chen and W. Luo, *Adv. Energy. Mater.*, **2018**, 8, 1703489.
30. H. Xu, J. Wan, H. Zhang, L. Fang, L. Liu, Z. Huang, J. Li, X. Gu and Y. Wang, *Adv. Energy. Mater.*, **2018**, 8, 1800575.
31. T. Liu, P. Li, N. Yao, G. Cheng, S. Chen, W. Luo and Y. Yin, *Angew. Chem. Int. Ed.*, **2019**, 58, 4679-4684.
32. J. Yu, W. J. Li, H. Zhang, F. Zhou, R. Li, C. Y. Xu, L. Zhou, H. Zhong and J. Wang, *Nano Energy*, **2019**, 57,

222-229.

33. H. Tabassum, W. Guo, W. Meng, A. Mahmood, R. Zhao, Q. Wang and R. Zou, *Adv. Energy Mater.*, **2017**, 7, 1601671.
34. M. Q. Wang, C. Ye, H. Liu, M. Xu and S. J. Bao, *Angew. Chem. Int. Ed.*, **2018**, 57, 1963-1967.
35. X. Zhang, X. Yu, L. Zhang, F. Zhou, Y. Liang and R. Wang, *Adv. Funct. Mater.*, **2018**, 28, 1706523.
36. F. Sun, Y. Wang, L. Fang, X. Yang, W. Fu, D. Tian, Z. Huang, J. Li, H. Zhang and Y. Wang, *Appl. Catal. B. Environ.*, **2019**, 256, 117851.
37. B. Liu, Y. F. Zhao, H. Q. Peng, Z. Y. Zhang, C. K. Sit, M. F. Yuen, T. R. Zhang, C. S. Lee and W. J. Zhang, *Adv. Mater.*, **2017**, 29, 1606521.
38. D. Yoon, J. Lee, B. Seo, B. Kim, H. Baik, S. H. Joo and K. Lee, *Small*, **2017**, 13, 1700052.
39. P. Wang, K. Jiang, G. Wang, J. Yao and X. Huang, *Angew. Chem. Int. Ed.*, **2016**, 55, 12859-12863.
40. Y. Wang, Z. Liu, H. Liu, N. T. Suen, X. Yu and L. Feng, *ChemSusChem*, **2018**, 11, 2724-2729.
41. J. Creus, S. Drouet, S. Suriñach, P. Lecante, V. Collière, R. Poteau, K. Philippot, J. Garcia-Antón and X. Sala, *ACS Catal.*, **2018**, 8, 11094-11102.
42. K. Wang, Q. Chen, Y. Hu, W. Wei, S. Wang, Q. Shen and P. Qu, *Small*, **2018**, 14, 1802132.
43. Q. Lu, A. L. Wang, H. Cheng, Y. Gong, Q. Yun, N. Yang, B. Li, B. Chen, Q. Zhang, Y. Zong, L. Gu and H. Zhang, *Small*, **2018**, 14, 1801090.
44. Z. Liu, Z. Li, J. Li, J. Xiong, S. Zhou, J. Liang, W. Cai, C. Wang, Z. Yang and H. Cheng, *J. Mater. Chem. A*, **2019**, 7, 5621-5625.
45. Y. Wang, L. Chen, X. Yu, Y. Wang and G. Zheng, *Adv. Energy Mater.*, **2017**, 7, 1601390.
46. M. Lao, K. Rui, G. Zhao, P. Cui, X. Zheng, S. X. Dou and W. Sun, *Angew. Chem. Int. Ed.*, **2019**, 58, 1-7.
47. K. Gao, Y. Wang, Z. Wang, Z. Zhu, J. Wang, Z. Luo, C. Zhang, X. Huang, H. Zhang and W. Huang, *Chem. Commun.* **2018**, 54, 4613-4616.